www.czasopisma.pan.pl PAN POLSKA AKADEMIA NAUK www.journals.pan.pl

Arch. Metall. Mater. **62** (2017), 2B, 1197-1200

DOI: 10.1515/amm-2017-0176

S. YANG*, J.-GON. KIM*#

MAGNETIC PROPERTIES OF $(Ni_a\text{-}Zn_b)_X\ Cu_{1\text{-}X}$ FERRITE NANOPARTICLE FABRICATED BY SOL-GEL PROCESS

In future, more mobile devices with different frequencies will be used at the same time. Therefore, it is expected that the trouble caused by wave interference between devices will be further intensified. In order to prevent this trouble, investigation of selective frequency transmission or absorption material is required. In this paper, magnetic properties of nickel-zinc-copper ferrite nano powder was researched as wave absorber. $(Ni_a\text{-}Zn_b)_xCu_{1\text{-}x}Fe_2O_4$(NZCF) nanoparticles were fabricated by the sol-gel method. The influence of copper substitution on lattice parameter change was analyzed by X-ray diffraction (XRD), particle size was analyzed by scanning electron microscopy (SEM), and Magnetic properties analyzed by vibrating sample magnetometer (VSM). The NZCF and Nickel-zinc ferrite (NZF) lattice parameter difference was 0.028 Å and particle size was calculated as 30 nm with the XRD peak. The VSM results of $(Ni_{0.3}\text{-}Zn_{0.3})_{0.6}Cu_{1\text{-}0.6}Fe_2O_4$ annealed sample at 700°C for 3hous were 58.5 emu/g (M_s), 22.8 Oe (H_c). It was the most suitable magnetic properties for wave absorber in this investigation.

Keywords: Ni-Zn-Cu ferrite, nanoparticle, soft magnetic property, sol-gel

1. Introduction

Wave absorbers are expected to be applied to a multitude of the frequency range of next-generation vehicle and mobile communication devices, etc. Malfunctions are caused by wave interference inside or between devices. Therefore wave absorber materials were needed in order to eliminate unnecessary wave frequency [1-5]. In this study, we investigated the magnetic properties of Ni-Zn-Cu spinel ferrite as a wave absorber. Microparticle spinel ferrite absorption range is from tens to hundreds megahertz, and spinel ferrite is needed to expand the wave absorption range to gigahertz. The wave absorption range increases with the increase in initial permeability and saturation magnetization [6-8]. Saturation magnetization is decided by the interaction of tetrahedral and octahedral element magnetic moments, grain size, and composition of substituted elements. In general, Zn^{2+}ion occupy tetrahedral on A-site, Ni^{2+} and Zn^{2+} ion-occupied octahedral on B-site in the spinel structure [9]. Coercive force is influenced by substituting element, such as Ni, Co, Cu, and Zn, and the coercive force is influenced more by substituted Cu^{2+} ion on the octahedral site than substituted Ni^{2+} or Zn^{2+}ion on tetrahedral site. Coercive force is increased by increasing the Cu anisotropy on octahedral site with Jann-Teller effect [9]. Therefore, we analyzed magnetic properties of NZCF nanoparticles. NZCF nanoparticles $(Ni_a\text{-}Zn_b)_xCu_{1\text{-}x}Fe_2O_4$ (a = b, a + b = x, x = 0, 0.2, 0.4, 0.6, 0.8) ware fabricated by sol-gel process. The magnetic properties and crystal structure of NZCF nanoparticle was analyzed with X-ray diffraction (XRD), scanning electron microscopy (SEM), and a vibrating sample magnetometer (VSM).

2. Experimental

The composition of NZCF $(Ni_a\text{-}Zn_b)_x\ Cu_{1\text{-}x}\ Fe_2O_4$ (a = b, a + b = x, x = 0, 0.2, 0.4, 0.6, 0.8) was prepared by sol-gel process. Iron nitrate hydrate $Fe(NO_3)_3{\cdot}9H_2O$, Zinc acetate dehydrate $Zn(CH_3COO)_2{\cdot}2H_2O$, Nickel acetate hydrate $Ni(CH_3COO)_2{\cdot}XH_2O$, Copper acetate $Cu(CH_3COO)_2$ ware used as starting materials and mixed by the stoichiometric ratio in deionize water (D.I). Citric acid and ethylene glycol were added to the mixture. Then, the mixture acidity was adjusted to pH 6 by ammonia solution. The mixture was heated and refluxed at 85°C for 8hours. The sol was evaporated at 100°C until it was transformed to gel on hot plate. The gel was annealed in air at 400, 500, 600, 700, and 800°C for 3hours, and then it was cooled down to room temperature in the furnace. The crystal structure of the annealed powder was analyzed by XRD (Rigaku, smartLab, Cu Kα, λ = 0.15425 nm, 2θ = 20°~70°). The average particle size was calculated by the Eq. (1) from (311) peaks of the spinel structure [11].

$$D=\frac{0.9\lambda}{\beta\cos\theta} \tag{1}$$

D is the crystal size, λ is the X-ray wavelength, β the broadening of the diffraction peak and θ is the diffraction angle. Particle size and shape was investigated by SEM (JEOL, JSM-7800F) image. Saturation magnetization (M_s), Coercive force (H_c), Initial permeability (μ_i) was measured by VSM (Quantum Design, VersaLab VSM, ±3,000 Oe, room temperature).

* ADVANCED MATERIALS SCIENCE AND ENGINEERING, INCHEON NATIONAL UNIVERSITY, 119 ACADEMY-RO, YEONSU-GU, INCHEON, 22012 KOREA

Corresponding author: jyj309@inu.ac.kr

3. Results and discussion

XRD peaks of nickel-zinc ferrite (NZF) and NZCF series are demonstrated in Fig. 1. The peak patterns of the samples have the same shape in XRD patterns of the NZF and NZCF series. This means that the lattice structure of the samples are the same. However, we noticed that the NZCF peak shifted to the right from NZF peak in Fig. 2. The peak shift was influenced by the change in lattice parameter in the spinel structure, and this change of lattice parameter was caused by Cu substitution on the Ni-Zn site. The change of the NZCF series lattice parameter is presented in Fig. 3 and Table 1. The Lattice parameter of NZCF 02 ($(Ni_{0.4}\text{-}Zn_{0.4})_{0.8}\ Cu_{1\text{-}0.8}\ Fe_2O_4$) was 8.406 Å, NZCF 04 was 8.403 Å, NZCF 06 was 8.384 Å, and NZCF 08 was 8.382 Å, indicating that the lattice parameter of NZCF had an inversely proportional relationship to Cu content. The lattice parameter was changed by difference ion radius of Ni-Zn and Cu. In particular, the change in the lattice parameter was affected by Zn^{2+} contents. Zn^{2+} ions ware substituted with Fe^{2+} ions on the tetrahedral in (100) spinel structure. Thus, Zn^{2+} ions entered into the tetrahedral in A-site, which swelled the lattice and enlarged the lattice parameter.

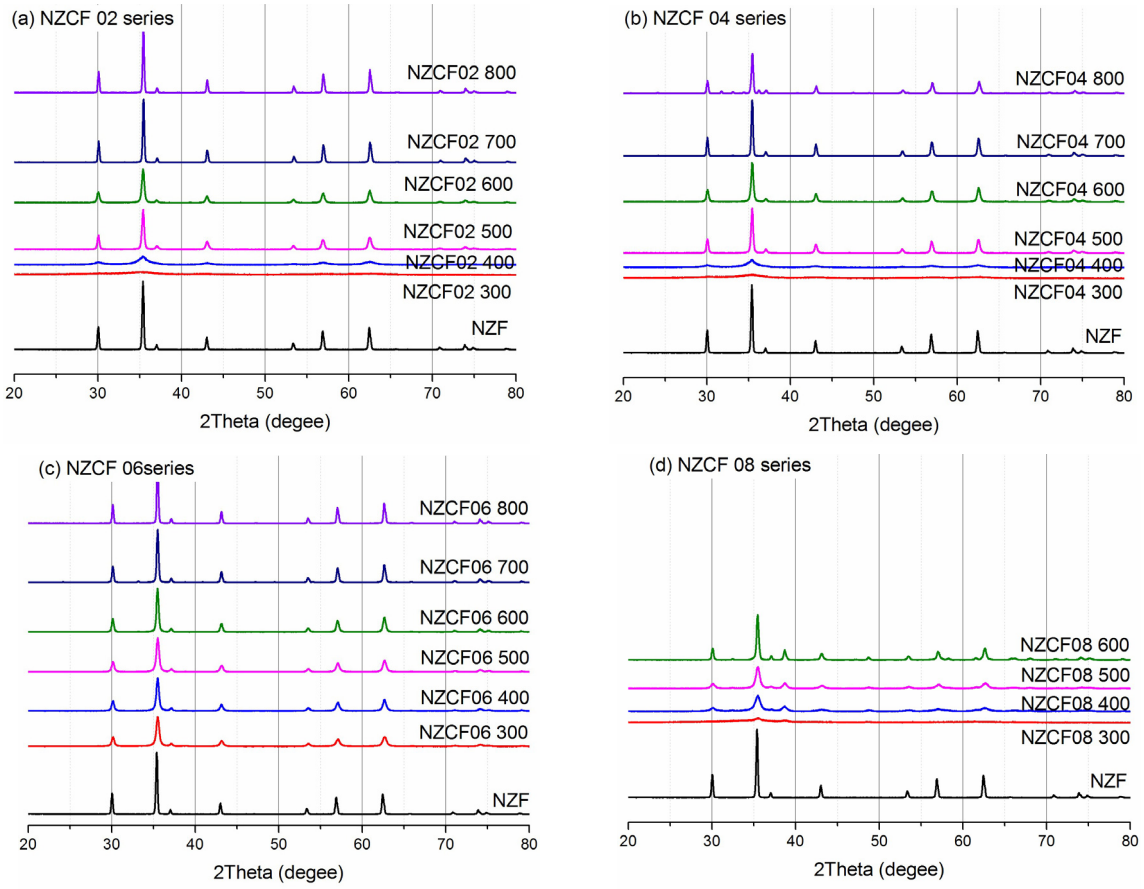

Fig. 1. XRD peak of each series. (a)NZCF 02, (b) 04, (c) 06, (d) 08

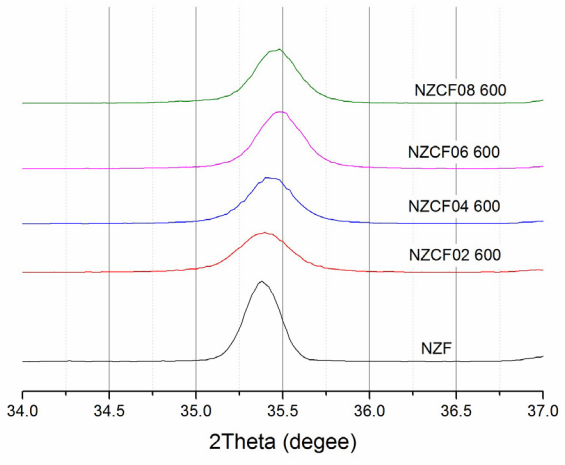

Fig. 2. NZCF series XRD peaks shift than NZF

TABLE 1

Lattice parameter (Å)

Series	Annealing Temperature (°C)				
	400	500	600	700	800
NZCF 02	8.429908	8.406083	8.408172	8.399145	8.399197
NZCF 04	8.399547	8.403199	8.400767	8.391086	8.38848
NZCF 06	8.388300	8.384436	8.389522	8.386922	8.387524
NZCF 08	8.34889	8.381678	8.37996		

The Particle size of calculated by formula (1) was presented on Table 2, Fig. 4 and NZCF 06 series SEM image is demonstrated in Fig. 5. Annealed NZCF at 400°C for 3hous, it showed a broad XRD pattern in Fig. 1, and it seem to show the NZCF precursor in Fig. 5a. The NZCF spinel structure began to be formed from 500°C.

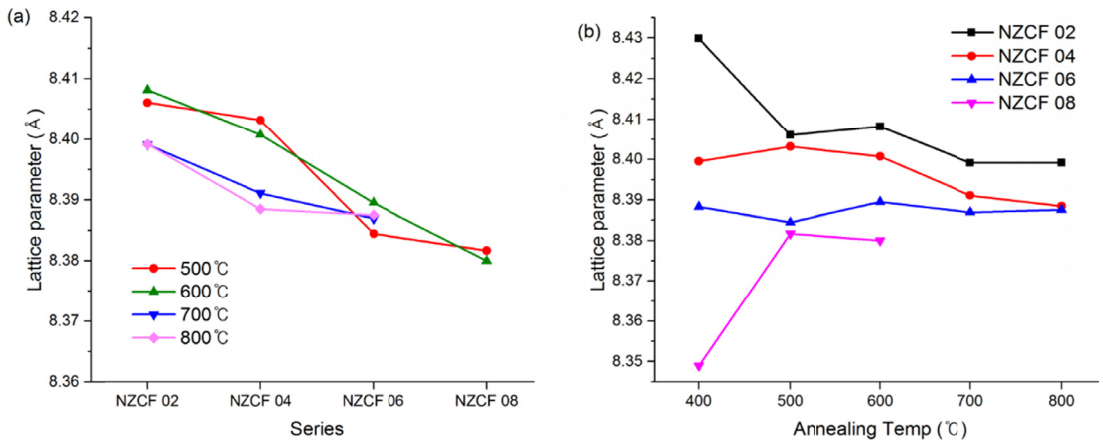

Fig. 3. Lattice parameter (a) Align of series (b) Align of Temperature

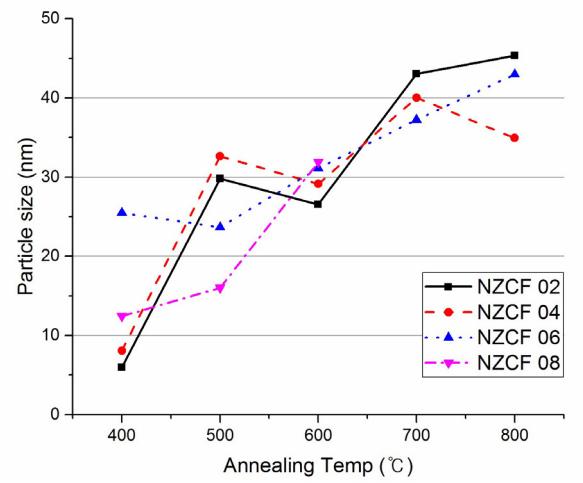

Fig. 4. Particle size calculated result

TABLE 2

(311) Particle size calculation result

Temp. (°C)	NZCF 02	NZCF 04	NZCF 06	NZCF 08
400	5.98	8.06	25.47	12.44
500	29.83	32.62	23.67	16.01
600	26.55	29.13	31.11	31.90
700	43.03	40.02	37.24	
800	45.34	34.93	42.97	

VSM results are summarized in Table 3, and Fig. 6. NZCF 06, NZCF 08 had relativity lower saturation magnetization values of 47.26 emu/g and 21.22 emu/g, respectively. This was because the B-site net magnetic moment was reduced by moving the Fe^{2+} ion of the octahedral site to the tetrahedral site and increased when the content of substituted Ni^{2+}, Cu^{2+} ions on the octahedral site was high [10].

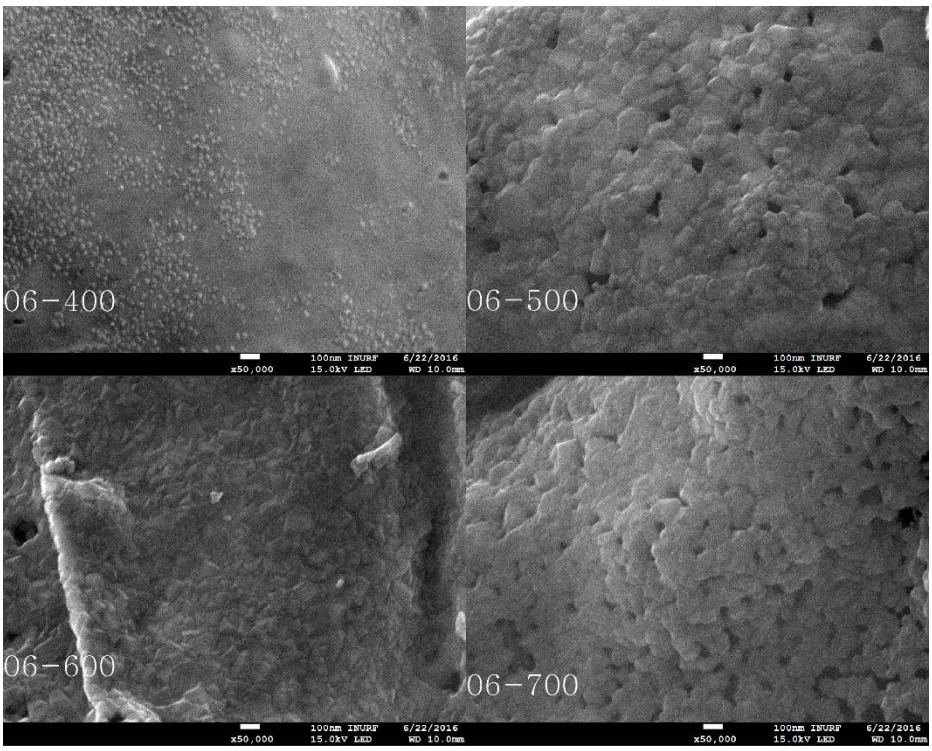

Fig. 5. Change of NZCF 06 series particle size (SEM : X50,000)

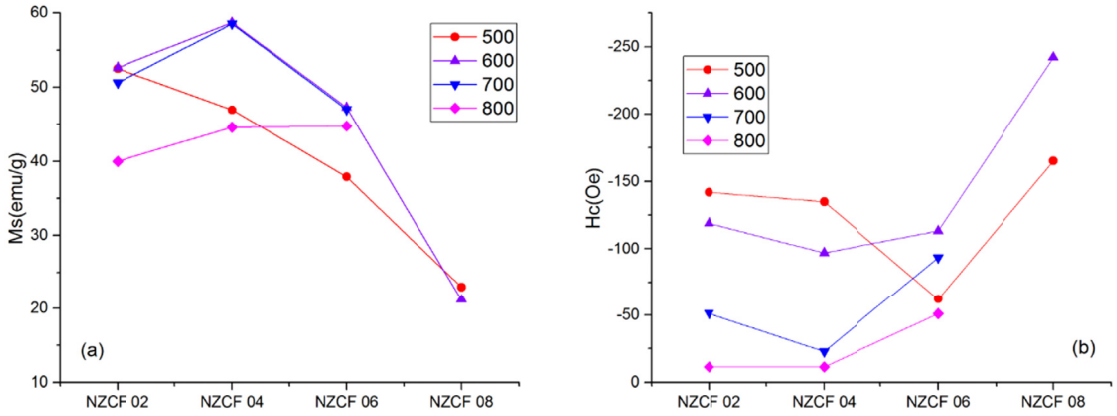

Fig. 6. Magnetic properties (a) Ms (b)Hc

TABLE 3

Magnetic properties of NZCF 02, 04, 06, 08 series

Temp. °C	Properties	NZF	NZCF 02	NZCF 04	NZCF 06	NZCF 08
400	Ms (emu/g)		17.23	22.38	18.5	18.15
	Hc(Oe)		–51	–78	–47.8	–183
	μi		0.01803	0.03073	0.02553	0.01545
500	Ms		52.52	46.94	37.89	23
	Hc		–142	–135	–62.25	–165.3
	μi		0.05438	0.03837	0.04669	0.02556
600	Ms		52.63	58.7	47.26	21.22
	Hc		–119	–96.9	–113.3	–242
	μi		0.04357	0.05413	0.054	0.01184
700	Ms		50.6	58.53	47	
	Hc		–51.3	–22.8	–93.47	
	μi		0.0175	0.0256	0.018	
800	Ms	53	40	44.6	44.76	
	Hc	–35	–11.4	–11.4	–51.07	
	μi	0.0956	0.0077	0.0311	0.0737	

NZCF 08 annealed at 600°C had a relativity large coercive force, because of it has a large magnetocrystalline anisotropy caused by the stress of lattice distortion from Jann-Teller effect. Coercive force was influenced by magnetic anisotropy [9].

4. Conclusions

NZCF $(Ni_a\text{-}Zn_b)_x\,Cu_{1-x}\,Fe_2O_4$ (a = b, a + b = x, x = 0, 0.2, 0.4, 0.6, 0.8) nanoparticles ware fabricated by sol-gel process. The main factor of the change in lattice parameter was Zn^{2+}ions that ware substituted on a-site tetrahedral of the spinel structure. Therefore, as copper content increased, the lattice parameter of NZCF decreased in the NZCF $(Ni_a\text{-}Zn_b)_x\,Cu_{1-x}\,Fe_2O$ system. A comparison of the lattice parameters of NZCF 02 and NZCF 08 annealed at 600°C 3hours revealed that there was a radius difference of 0.028Å. This difference was caused by the substituting Zn^{2+} ion on the tetrahedral site in the spinel structure.

High quality soft magnetic wave absorption materials must have properties of high saturation magnetization and low coercive force. In this study, NZCF 04, 06 series of 500~700°C had high a high saturation magnetization value and a comparatively small coercive force value. Therefore, this NZCF 04, 06 series of 500~700°C could be a wave absorber material. Saturation magnetization and coercive force was mainly decided interaction of Fe^{2+} ions and substituted elements and magneto crystalline anisotropy. NZCF 04 700°C had 58.5 emu/g and 22.8 Oe, making it the most suitable for wave absorber in this investigation.

Acknowledgments

This work was supported by Incheon National University (International Cooperative) Research Grant in 2016.

REFERENCES

[1] M.E. McHenry, M.A. Willard, D.E. Laughlin, Prog. Mater. Sci. **44**, 291-433 (1999).
[2] M.E. McHenry, D.E. Laughlin, Acta Mater. **48**, 223-238 (2000).
[3] Y. Yoshizawa, Scripta Mater. **44**, 1321-1325 (2001).
[4] Z. Stokłosa, J. Rasek, P. Kwapulinski , G. Badura, G. Haneczok, L. Pajak, J. Lelatko, A. Kolano-Burian, J. Alloy. Compd. **509**, 9050-9054 (2011).
[5] G. Herzer, Acta. Mater. **61**, 718-734 (2013).
[6] J.H. Nam, H.H. Jung, J.Y. Shin, J.H. Oh, IEEE. T. Magn. **31**, 3985-3987 (1995).
[7] C.S. Kim, W.C. Kim, S.Y. An, S.W. Lee, J. Magn. Magn. Mater. **215-216**, 213-216 (2000).
[8] T. Nakamura, J. Magn. Magn. Mater. **168**, 285 (1997).
[9] F.S. Tehrani, V. Daadmehr, A.T. Rezakhani, R.H. Akbarnejad, S. Gholipour, J. Supercond. Nov. Magn. **25**, 2443-2455 (2012).
[10] J.C. Aphesteguy, A. Damiani, D. DiGiovanni, S.E. Jacobo, Physica. B **404**, 2713-2716 (2009).
[11] P. Scherrer, Mathematisch-Physikalische Klasse, **2**, 98-100 (1918).